Engineering Structures 325 (2025) 119407

Contents lists available at ScienceDirect

Engineering Structures

journal homepage: www.elsevier.com/locate/engstruct

# Experimental investigation of the bearing capacity between short hollow glass columns and a transparent thermoplastic interface material

Joseph Robert Yost [a], Matthew Cregan [b], Damon Bolhassani [c], Philipp Amir Chhadeh [d], Jens Schneider [e], Yao Lu [f], Masoud Akbarzadeh [f,g,*]

[a] Structural Engineering Teaching and Research Laboratory (SETRL), Villanova University, Villanova, PA, USA
[b] Hardesty, Hanover, New York City, USA
[c] ABC Lab, The Bernard and Anne Spitzer School of Architecture, The City College of New York, New York, NY, USA
[d] Institute of Structural Mechanics and Design, Technische Universität Darmstadt, Darmstadt, Germany
[e] Technische, Universität, Wien, Vienna, Austria
[f] Polyhedral Structures Laboratory, Department of Architecture, Weitzman School of Design, University of Pennsylvania, Philadelphia, PA, USA
[g] General Robotic, Automation, Sensing and Perception (GRASP) Lab, School of Engineering and Applied Science, University of Pennsylvania, Philadelphia, PA, USA

ARTICLE INFO

*Keywords:*
Hollow glass unit
Compression-dominant glass structures
Polyhedral glass structures
3D/polyhedral graphic statics

ABSTRACT

In this research study, the fracture strength of flat 10 mm thick annealed glass sheets having an abrasive water-jet cut surface and bearing against a transparent interface material is experimentally investigated. The transparent interface material is necessary to provide axial-compressive force continuity in modular compression-dominant all- glass shell structures. A series of short glass columns were tested in axial compression under a variety of load cases, which included cyclic, creep, and monotonic-to-fracture loading. A target glass fracture bearing stress of 36.6 MPa is identified and represents an upper bound bearing stress for annealed glass compression members failing in a flexural buckling mode. The study concludes the transparent thermoplastic material, known as Surlyn, was able to achieve a fracture strength that exceeds the target value and that the fracture strength is not affected by cyclic or creep loading. Consequently, column-related failure limit states will occur before glass fracture is associated with interface bearing. Glass fracture occurs in Type-I mode, reflecting the presence of interface tensile stress. Furthermore, the monotonic bearing stiffness in the service range of 5 to 15 MPa is increased by 20 % and 16 % for samples subjected to cyclic and creep loading, respectively, relative to monotonic-only samples.

## 1. Introduction

The use of glass as a material for primary compression members requires design for failure limit states associated with column action. The corresponding capacity, $P_{col}$, considers failure limited by the material's compression strength or stability failure by buckling, which includes flexural, torsional, flexural-torsional and local buckling. However, each of the limit states associated with column strength ($P_{col}$) assumes the axial load at which the column fails is achievable before local fracture of the glass at the locations of column support ($P_{cr}$). These strength limits reflect detailing at the support locations of an isolated column, where equilibrium and load-path necessitate that axial compression force enter the column cross-section via bearing with another member or structural material. For steel and concrete compression members, this is rather simple and involves column framing at support locations with similar materi- als. Thus, steel-on-steel, concrete-on-concrete or steel-on-concrete connection detail- ing effectively allows force to enter the column with little concern for support location fracture limit states. This is not the case with glass, where load introduction to the column cross-section must consider local fracture limit states associated with bearing stresses on the column cross-section. Clearly, for glass columns of normal slenderness, direct contact with steel, concrete or any other hard substance will result in failure by local fracture ($P_{cr}$) well before the limit states associated with column

* Corresponding author at: Polyhedral Structures Laboratory, Department of Architecture, Weitzman School of Design, University of Pennsylvania, Philadelphia, PA, USA.
*E-mail addresses:* joseph.yost@villanova.edu (J.R. Yost), mbolhassani@ccny.cuny.edu (D. Bolhassani), chhadeh@ismd.tu-darmstadt.de (P.A. Chhadeh), schneider@ismd.tu-darmstadt.de (J. Schneider), yaolu61@design.upenn.edu (Y. Lu), masouda@design.upenn.edu (M. Akbarzadeh).

https://doi.org/10.1016/j.engstruct.2024.119407
Received 4 July 2024; Received in revised form 31 October 2024; Accepted 25 November 2024
Available online 12 December 2024

action ($P_{col}$) are achieved. Thus, an interface material is required between the glass column cross- section and supporting elements, the function of which is to smooth out local bearing stress concentrations on the glass's loaded edge so that fracture capacity ($P_{cr}$) exceeds.

column strength ($P_{col}$).

As built examples of isolated glass columns serving a primary structural function are few, and this reflects the coupled effect of glass's brittle nature together with limited opportunity for load redistribution in compression critical structural elements. How- ever, in the literature a few prominent examples are found and include the town hall in Saint Germain-en-Laye France (Fig. 1a, [1]), an office building in Nordborg Den- mark (Fig. 1b, [2]) and a cafe´in Go¨ppingen Germany (Fig. 1c, [3]). In each of these examples, an interface material is necessary and plays a central role in the effective function of glass as the material for primary compression members. Specifically, load-introduction in all three cases (St. Germain, Nordborg, and Go¨ppingen) was re- ported to be via an intermediary material of neoprene strips [4].

Moreover, direct contact between glass and other rigid structural materials is to be avoided in various applications where glass is used for structural purposes. For ex- ample, point-supported mechanical connections are often used between neighboring glass panels (Fig. 2a) and between glass and other structural elements (Fig. 2b). Typically, rigid stainless steel skeletal contraptions, known as spider assemblies, are bolted to the glass. For in-plane loading, the bolts act in shear and, in doing so, must bear against the glass through an interface material to prevent direct glass-on-bolt steel.

contact (Fig. 2c). This interface mandate is required by CEN/TS 19100 – 3 [5], with interface material typically aluminum or a synthetic such as PTFE, Polyamide, Polychloroprene, Silicone, etc. [6]. In curtain wall support systems, PVC inserts are generally used to transfer the gravity load associated with the glass self-weight to sup- porting elements. In general, the material through which force enters and exits the glass plays a central role in achieving the strength potential of a given structural glass unit (i.e., beam, column, plate, etc.).

In summary, the study of bearing force transfer between glass and an interface ma- terial is ultimately concerned with understanding how these two materials interact on a micro-scale. At this scale, the surface features of the glass interact with the ma- terial properties of the interface material and determine the glass's fracture strength. Therefore, the interface material's function is to micro-deform with the surface irregularities in the glass, thereby limiting local stress concentrations at the locations of micro-contact. The interface material uniformly distributes the bearing force over the macro-scale glass cross-section, eliminating local peaking stress concentrations at the glass surface texture irregularities. One can easily visualize that a rigid material, such as steel or concrete, in contact with glass cannot deform with the glass surface irregu- larities, thereby creating local stress concentrations that ultimately lead to glass fracture at bearing stress levels well below the member's compression strength.

### 1.1. Research context and scope

In the current study, the need for a transparent interface material for glass compression members is motivated by developing a proposed compression-dominant structural glass system that is entirely transparent and modular in assembly. In the proposed system, large compression-dominant transparent shell structures are created by assembling smaller individual hollow-glass units (HGU). In this proposal, an HGU is a rigid three-dimensional compression member made from top and bottom glass deck plates that resist in-plane compression and are connected to acrylic side plates. A two-sided transparent structural tape known as 'very high bond' tape, or simply VHB tape [9] is used to make the deck plate to side plate connections. A typical HGU is shown in Fig. 3a, and a small-scale 3 m span prototype assembly of HGUs into a compression- dominant shell structure is shown in Figs. 3b and 3c. The current objective of this novel structural system is the construction of a fully transparent 10 m pedestrian bridge, as described in Akbarzadeh et al. [10].

The geometry of the fully assembled shell structure into a compression-dominant form is found using three-dimensional polyhedral graphic statics, as described in Ak- barzadeh [11]. Full details related to the assembly methodology of an individual HGU.

and the construction of the 3 m prototype can be found in Lu et al. [12]. Details and results related to axial compression testing of individual HGUs can be found in Yost et al. [13]. Significant in the aforementioned discussion is that the deck plates are 10 mm thick single-layer float glass, and the required deck plate geometry is made using 5-axis abrasive waterjet cutting technology. Furthermore, flexural buckling of the HGU deck plates subjected to in-plane compression was achieved by Yost et al. [13] using an ori- ented strand board (OSB) as an interface material in the experimental program. In this study, the OSB-to-glass bearing stress at flexural buckling failure ranged between 30.1 and 36.6 MPa. The stated bearing stress range corresponds to column action strength because the OSB effectively prevented glass fracture

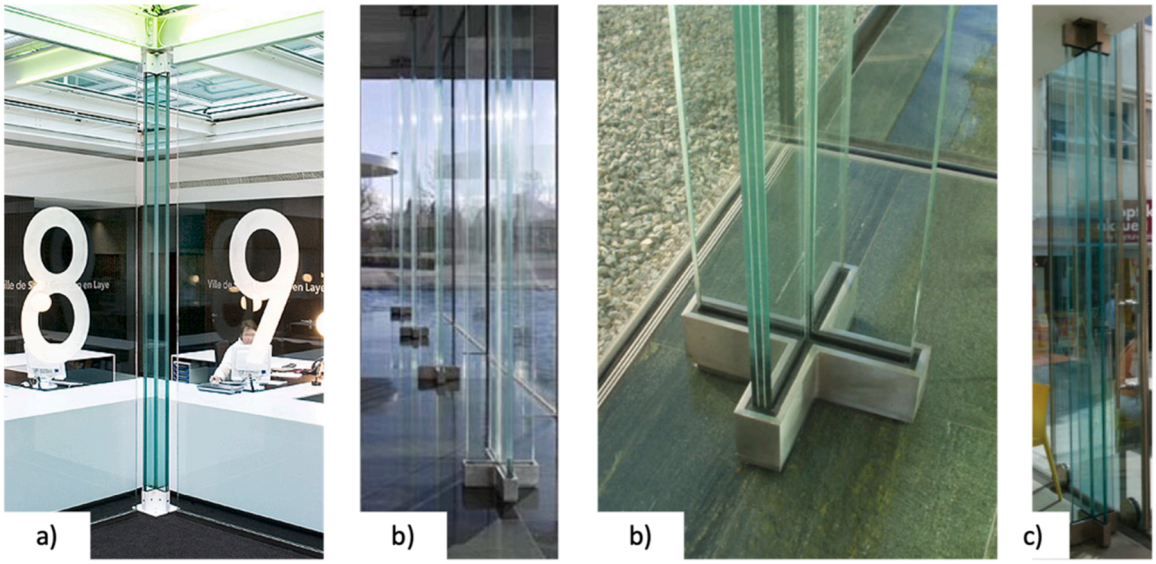


**Fig. 1.** Glass as a primary structural compression member: (a) St. Germain France [1], (b) Nordborg Denmark [2], (c) Göppingen Germany [3].

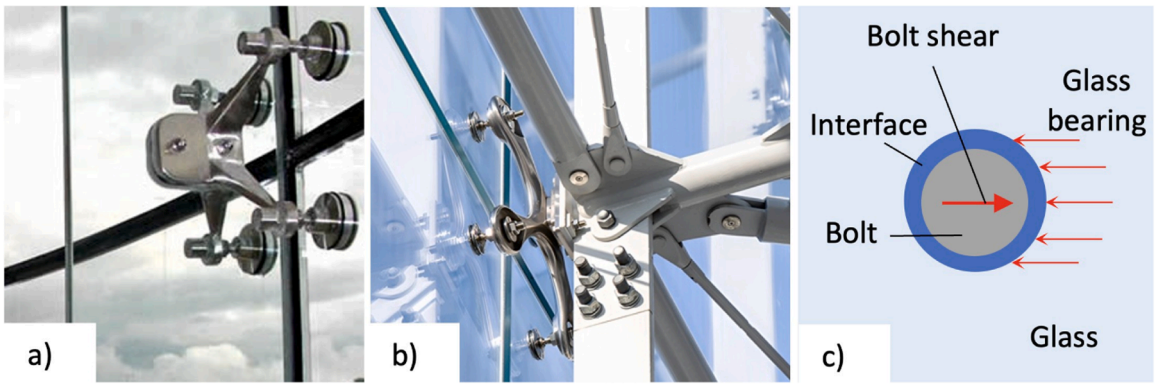


**Fig. 2.** Point supported glass: a) glass panel-to-panel connection [7], b) glass-to-steel connection [8], c) Force transfer at bolt.

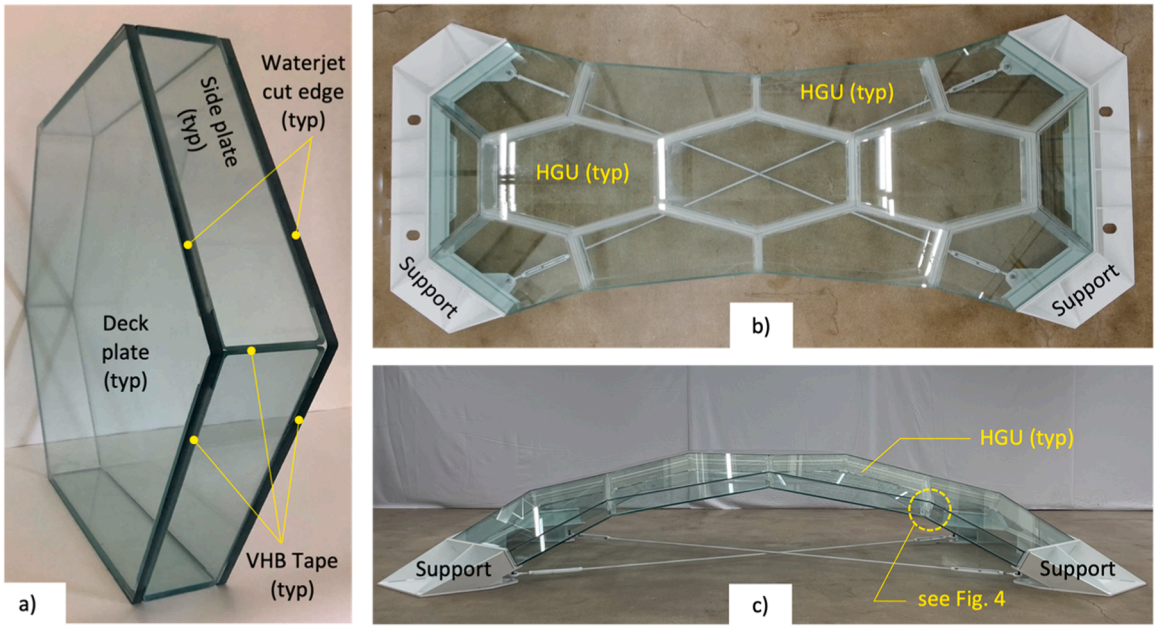


**Fig. 3.** Proposed modular compression-dominant structural glass system: a) Individual hollow glass unit (HGU), b) 3 m prototype top view, c) 3 m prototype side view.

on the loaded glass edge. This range will be a central target in the current research study.

To achieve the strength potential of the proposed compression-dominant modular glass system, it is necessary to effectively transfer the in-plane deck plate compression force between neighboring HGUs, as is shown in the joint detail of Fig. 4. Glass- on-glass contact between neighboring deck plates must be avoided, which mandates an interface material to facilitate in-plane deck plate compression force continuity across the HGU joint with no local glass fracture. The interface material must be transparent and conservatively able to develop a target bearing stress of 36.6 MPa before glass fracture, an upper-bound limit for the range referenced, and a lower-bound limit for the current study. This target is also specific to float glass with an abrasive water-jet cut edge. Additionally, for the proposed pedestrian bridge application, the state of bearing stress should consider time-related dependence, such as load cycling and creep.

In conclusion, the current research study aims to find a transparent interface ma- terial that achieves glass fracture at a lower bound bearing stress of 36.6 MPa. This target is achieved with the consideration of load cycling and creep. Preliminary mate- rial selection considered four transparent materials: Acrylic, Polyvinylchloride (PVC), Polycarbonate, and Surlyn. From trial monotonic testing of these four materials, only Surlyn was able to achieve the target fracture stress of 36.6 MPa (see Yost et al. [14]). Consequently, Surlyn was selected as the interface material for continued investigation, and the execution of a detailed experimental program is the objective of the current re- search study. It is also important to note that this research study and associated findings.

are significant in the broader generic need to effectively transfer force through bearing into the glass so that local fracture is absent and global member strength limit states are achieved.

### 1.2. Related Literature Review

The primary research scope of this paper is related to the need and function of interface materials for glass in compression and having bearing contact stress with other structural materials, including glass. Existing literature directly related to this scope is limited and in most publications this topic is secondary and included more to describe an experimental setup. Nonetheless, here there is valuable content related to the breadth of different material and surface finishing details used to serve the common purpose of preventing cracking by diluting bearing stresses on glass surfaces. Some examples follow.

Sanders et al. [15] investigated the strength of bolted annealed glass subjected to in-plane loading and having waterjet and drilled holes.

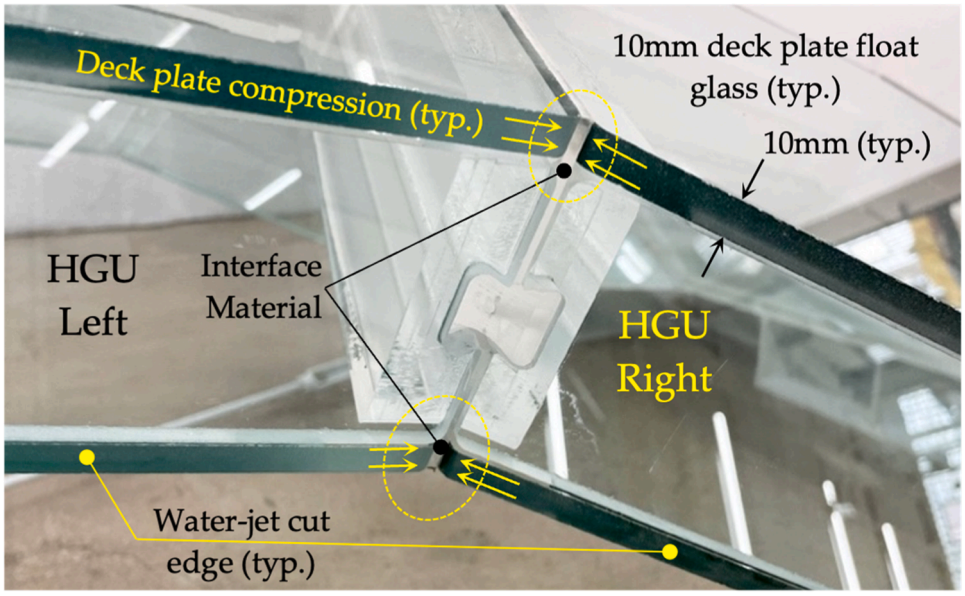


**Fig. 4.** HGU joint connection detail.

They found the failure load for waterjet cut holes was significantly lower than for drilled h oles. Their research also.

showed a similar finding for annealed glass loaded in bending with both waterjet cut and drilled holes. Jan Wurm [16] shows that the bearing force transfer from glass to an elastomeric substrate interface has a Shore-A hardness of 60 to 80. Experimental research by Oikonomopoulou [17] used lead as the interface material between bundled glass compression members and the top and bottom support locations. Their con- clusions state that lead as an interface material effectively eliminates cracking on the bearing surface of the glass. Kamarudin et al. [18] investigated circular glass columns in single and bundled configurations with 4 mm thick neoprene rubber pads as an inter- face between glass and load/support assemblies. For low slenderness columns, the first crack occurred at the bottom support with failure by progressive glass crushing at loads of 1.0 and 4.9 times that at the first crack. However, no cracking occurred at the sup- ports for high slenderness samples, and failure occurred by flexural buckling. Aiello et al. [19] refer to a transparent thermoplastic sheet as the interface between the glass column and the test machine. In the work by Kalamar et al. [20], square hollow glass columns were tested in axial compression with polyamide pads used as an interface be- tween glass and the load and support assemblies. Initial results showed cracking at the column base at a force and bearing stress of 72 kN and 20 MPa, respectively. Failure ultimately occurred at 95 kN by extension of the base cracks. Subsequent samples were modified with a thin layer of fine sand between the polyamide pads and load/support assemblies. Results were ineffective, and initial cracking again occurred on the edge of the glass at bearing stresses between 20 and 22 MPa.

## 2. Experimental program

The experimental program was designed to measure the fracture strength of an- nealed glass loaded in axial compression on an abrasive water-jet cut edge in a bearing with Surlyn acting as an interface material. Samples were sized as short glass columns with very low slenderness and no opportunity for stability-related failure limit states. A typical sample is shown in Fig. 5 and consists of four glass plates, including two col- umn plates (102 ×102 mm) stiffened by two diaphragm plates (95×80mm). All plates were single layers of 10 mm thick annealed glass with a 5 mm radius fillet, and all.

edges were cut using an abrasive water jet. The connection between the column and diaphragm plates was made using a 1 mm thick two-sided structural tape manufactured by 3 M, known as Very High Bond (VHB) tape [9]. Surlyn sheets 3 mm thick were placed on top and bottom between column plates. With this placement, the Surlyn out- side loaded edge was a free surface, and the inside loaded edge was a continuum of interface material. It should be noted that this is the same arrangement as the interface material between neighboring HGUs in the proposed structural system, as shown in Fig. 4.

Surlyn is a clear thermoplastic ionomer resin first synthesized by the DuPont cor- poration in the 1960s. As an ionomer it is a thermoplastic polymer material having both covalent and ionic bonds, and with

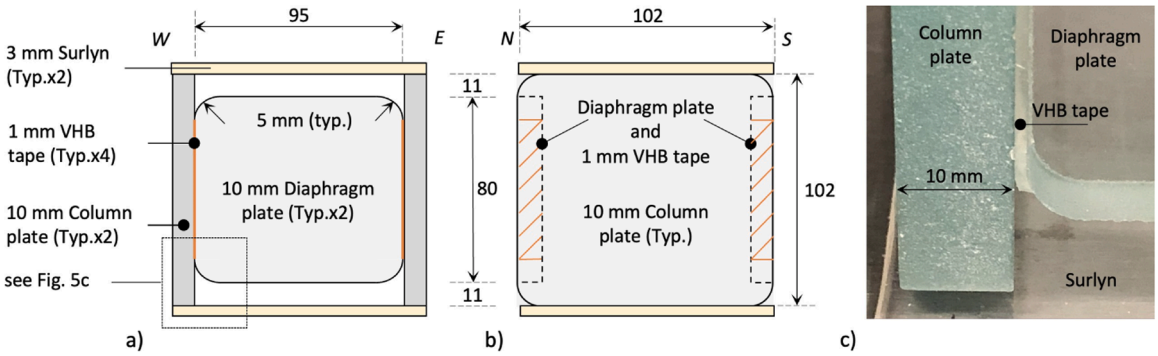


**Fig. 5.** Typical sample details. a) EW Elevation, NS Elevation, c) Connection View.

properties influenced by the ionic bonding. The chemical resistance, melting range, density, and basic processing characteristics of Surlyn are similar to those of ethylene-based copolymers, but it has better low-temperature impact toughness, abrasion, chemical resistance, transparency, and clarity, melt strength, and adhesion to other products (such as polyurethane and metal or glass). Surlyn ionomers offer high clarity, high gloss, oil and grease resistance, puncture re- sistance, scratch resistance, excellent hot tack strength, and superb thermoformability. Surlyn can be processed using conventional extrusion and injection equipment to create various shapes or sheets, and it has been used for many years in applications related to packaging, orthotics/prosthetics, golf ball skin, and sports equipment. In this research, 3.175 mm thick Surlyn Grade 8940 sheets manufactured by the DOW Corporation were cut to the size as shown in Fig. 5. Typical material properties for Surlyn Grade 8940,

as provided by the manufacturer [21], are as follows: Specific Gravity 0.95, Hardness Shore D 65, Flexural Modulus at Room Temperature 350 MPa, Room Temperature Tensile Strength at Yield and Break 15 and 33 MPa, respectively, Melting Point 94 oC, Freeze Temperature 59 oC and Haze at 6.35 mm (0.25 in.) is 5 %.

All short glass column samples were tested in a Material Test System (MTS) servo- hydraulic controlled test machine. The load and support apparatus is shown in Fig. 6 and consists of a spherical bearing secured to a stationary support at the top and a steel load frame connected to the hydraulic actuator at the bottom. Precision ground 12 mm thick steel plates were placed on top and bottom between the Surlyn and spher- ical bearing (top) and steel frame (bottom). Vertical displacement between the inside surfaces of the precision ground steel plates was measured by four 15 mm range po- tentiometers placed between the precision ground steel plates and in all four sample corners (NE, NW, SE, SW). Neglecting axial deformation in the glass, this vertical dis- placement represents the total bearing deformation in two Surlyn sheets. Applied load, MTS displacement, and potentiometer displacements were measured by a 16-bit data acquisition system.

In defining how the test samples would be loaded to fracture, it was considered that load cycling and creep loading could potentially affect the glass fracture strength in the bearing. The reasoning was that micro-scale crack formation and growth to a critical size could be accelerated by time-related load effects. For example, load cycling and sustained load could potentially have a local prying effect on crack growth, accelerating its formation to a critical size at which point fracture occurs. For this reason, three dif- ferent load cases (LC) were used during testing and include LC1) 100,000-cycle cyclic phase (CY) followed by 12 hr. creep phase (CR) followed by monotonic failure phase (MF), LC2) 40 hr. creep phase (CR) followed by monotonic failure phase (MF), and LC3) Monotonic to failure only phase (MF). The three load cases and corresponding sample identifications are graphically depicted in Fig. 7. The cyclic phase (desig- nated CY in LC1) consisted of 100,000 load cycles at 1 Hz between bearing stresses of 5 and 15 MPa. This bearing stress range corresponds to that expected from dead load (D) and dead load plus live load (D+L), respectively, in the proposed pedestrian bridge application. Data acquisition during the cyclic phase consisted of recording 2 cycles of data every 200 cycles at a data recording rate of 100 Hz. The creep phase (designated CR in LC1 and LC2) consisted of sustained load at 5 MPa (or D) for a duration of 12 h (LC1) or 40 h (LC2). During creep loading data was acquired continu- ously at a rate of 0.5 Hz. Monotonic loading to failure (designated MF) followed creep loading for LC1 and LC2, and was the entirety of LC3. During MF load was applied in displacement control at a rate of 0.10 mm/min until glass fracture occurred, after which the sample was unloaded. During MF data acquisition was continuous at 10 Hz. Finally, all tests were run under normal ambient indoor temperature and humidity con- ditions. Specifically, using a thermocouple located at the testing site, temperature was continuously recorded by the data acquisition system during testing for all load cases. From this data, the temperatures during testing were very stable and ranged for all tests from an average minimum of 22.6 C, to an average maximum of 24.3 C with an overall average of 23.4 C.

## 3. Test results

Test results are presented firstly as behavior measured during the time-dependent load phases, which include cyclic and creep loading in LC1 (CY+CR) and creep only in LC2 (CR only). This is followed by the monotonic failure test results for all load cases. In this way, the time-dependent results recorded during CY and CR represent.

Surlyn's response to the imposed load phases. This data is significant and necessary to understand the service limit state system response of glass compression members in contact with Surlyn as an interface material. The monotonic failure test results show the response of Surlyn to elevated bearing stress levels and, at glass fracture, what the glass strength in the bearing corresponds to the fracture limit state. From this data, the effects of cyclic and creep loading on glass fracture strength are explored by comparing the fracture strength of LC1 and LC2 samples with that of the LC3 samples. Importantly, for all test results, displacement is taken as the average of the four potentiometers located in the four plan-corners of the test sample and shown in Fig. 6b. This displacement represents the total Surlyn bearing deformation, which includes both the top and bottom sheets with a total thickness of

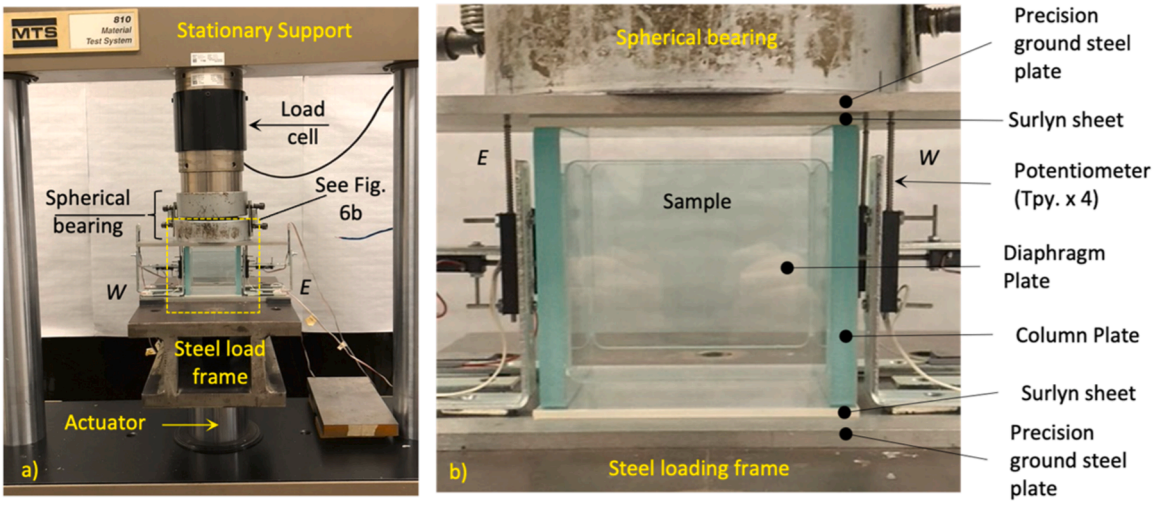


**Fig. 6.** Load & support details. (a) Test setup overview, (b) Sample in the test machine.

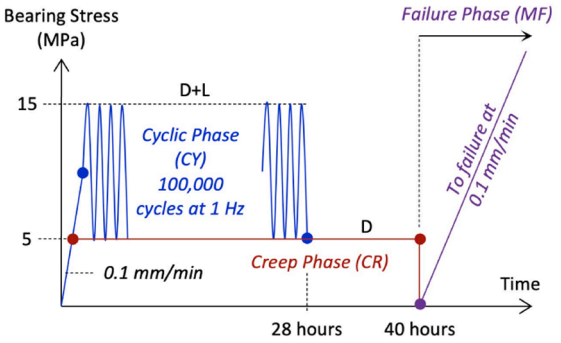


Load case and sample identification

| Load Case | Sample (ID) | Load Phase | | | N (#) |
|---|---|---|---|---|---|
| | | Cyclic (CY) | Creep (CR) | Failure (MF) | |
| Load Case 1 | CY+CR+MF | 100,000 cycles [1] | 12 hrs at D | Monotonic [2] | 6 |
| Load Case 2 | CR+MF | NA | 40 hrs at D | Monotonic [2] | 5 |
| Load Case 3 | MF | NA | NA | Monotonic [2] | 6 |

[1] between D and D+L at 1 Hz.

[2] to failure in displacement control at 0.1 mm/min.

**Fig. 7.** Load protocol and sample idenification.

6.35 mm.

### 3.1. Cyclic and creep test results

As mentioned, during cyclic loading force was applied at 1 *Hz*, and data was recorded for 2 s every 200 s, or 2 cycles every 200 cycles. Typical hysteresis be- havior at arbitrary cycles $n$ and $n + 200$ are shown in Fig. 8, where the displace- ments at minimum ($Y_D$) and maximum ($Y_{D+L}$) stresses are noted, and also the increases in these displacements ($\Delta Y_D$ and $\Delta Y_{D+L}$) with cycle number. As well in Fig. 8, the slope of a linear regression line for each 2-cycle data capture is designated $s_{cyclic}$ with units of *MPa/mm*. Note that multiplying $s_{cyclic}$ by the total Surlyn thickness of 2 * 3.175 *mm* = 6.35 *mm* equates to the slope of the hysteresis stress-strain response and represents Surlyn's cyclic bearing modulus, $k_{cyclic} = s_{cyclic}$ * 6.35 *mm*, with units *MPa*.

Note this bearing modulus ($k_{cyclic}$) is specific to the load frequency of 1 *Hz* and stress range of 5 to 15 *MPa*.

Figs. 9a and 9b show displacement versus time for Load Case 1 (LC1) and Load Case 2 (LC2) samples, respectively. The start time horizontally in Fig. 9a for CY (LC1) loading corresponds to the first two full load-cycle, and in Fig. 9b for LC2 this is the first full two seconds at creep load (i.e. D). From Fig. 9, the behavior is highly nonlinear in the beginning, with significant deflection growth during CY loading until about 10,000 cycles. Thereafter, the deflections $Y_D$ and $Y_{D+L}$ continue to

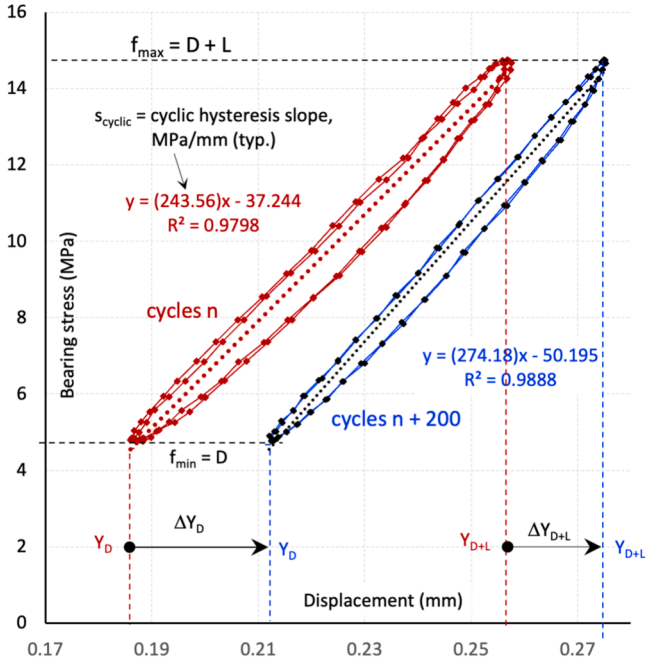


**Fig. 8.** Typical cyclic phase (CY) data capture (Sample CY+CR+MF-5 shown).

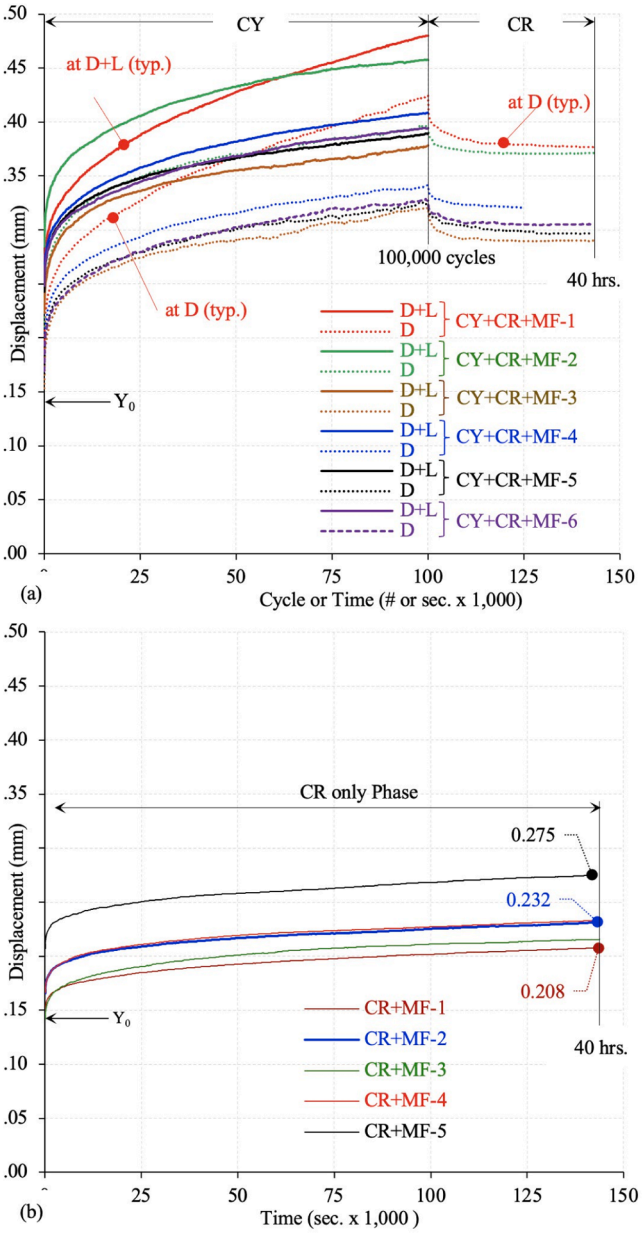


**Fig. 9.** Test result for a) Load Case 1, b) Load Case 2.

increase but at an increasingly flatter rate, becoming approximately linear at about 50,000 cycles.

and staying so till the end of CY loading at 100,000 cycles.

Importantly, there is still measurable deflection growth at the termination of CY loading for both $Y_D$ and $Y_{D+L}$. This would suggest that additional deflection growth would occur if load cycling continued beyond the imposed 100,000 cycles, however at an increasingly diminishing rate. For LC1 samples, the transition from CY loading to CR loading is represented by deflection $Y_D$ and shows a sharp inflection with a precipitous deflection decrease in the time interval at the start of CR. Thereafter, deflection decreases non-linearly, becoming approximately flat at the end of CR loading, or 40 h. This behaviour shows that some of the deflection increase that occurs during cyclic loading is recovered during creep loading. This recovery will be quantitatively investigated later in Fig. 10a.

From Fig. 9b for LC2 samples (creep loading only), there is a rapid and nonlinear increase in deflection growth in about the first 10,000 s, after which there is a smooth and gradual transition to a linear response becoming approximately constant at about 100,000 s. Thereafter, deflection increases at this constant rate until the termination of CR loading at 40 h. In general, at 40 h (i.e., end of CR), the LC1 $Y_D$ deflections exceed the LC2 deflections and represent the effects of CY loading.

A normalized interpretation of the deflection change shown in Fig. 9 is presented in Figs. 10a and 10b as the Change in Deflection relative to that corresponding to the initial cycle or time for LC1 and LC2, respectively. This normalized change is found as $\rho = 100\ \%*(Y_n–Y_0)/Y_0$, where $Y_0$ is the initial displacement, and $Y_n$ is the displacement at cycle $n$ or time $n$. In this way the differences in initial deflections noted in Fig. 9 are normalized, facilitating a more meaningful interpretation and comparison of test data. Results from Fig. 10 are quantitatively summarized in Table 1 for $\rho_D$ at 100,000 s and 40 h (LC1 and LC2), and $\rho_{D+L}$ at 100,000 s (LC1 only).

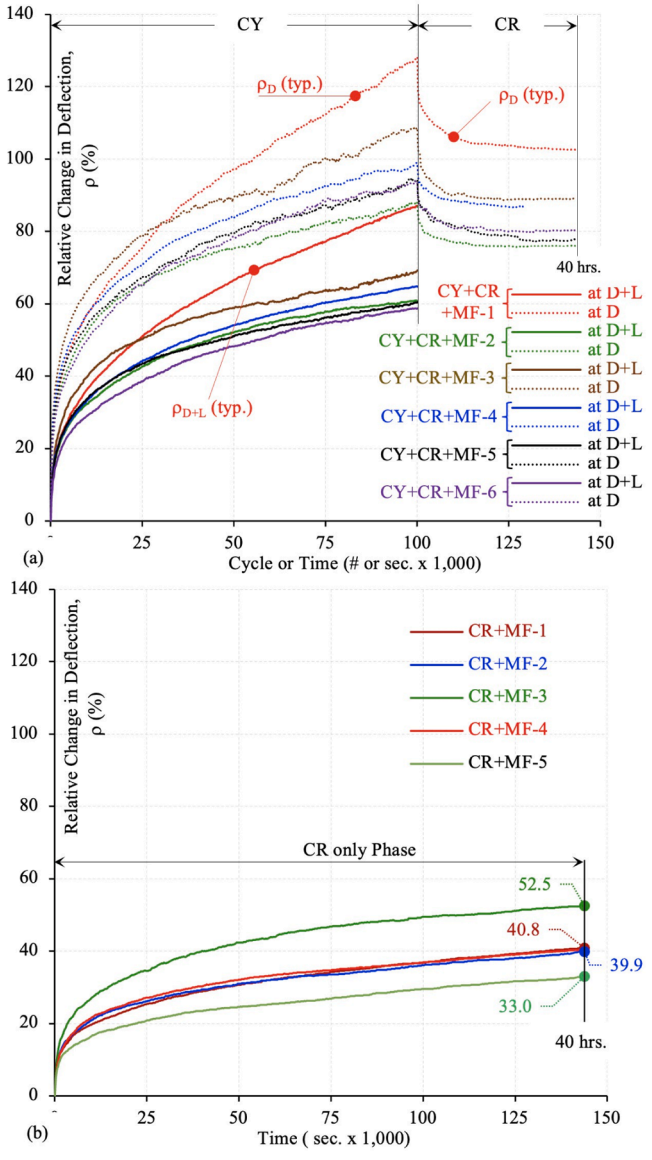


**Fig. 10.** Normalized deflection increase. a) Load Case 1, b) Load Case 2.

For LC1, Fig. 10a and Table 1 show that during CY loading, the relative change in minimum displacement ($\rho_D$) is significantly higher than the relative change in max- imum displacement ($\rho_{D+L}$). This is to be expected and represents residual deflection increase associated with load cycling to $f_{max}$ or $D + L$. Specifically, from Table 1 the average $\rho_D$ and $\rho_{D+L}$ at the conclusion of CY or 100,000 load cycles is 102 % and 67 %, respectively, or $\rho_D$ increases 35 % more than $\rho_{D+L}$. It is also noted in Fig. 10a that both $\rho_D$ and $\rho_{D+L}$ continue to increase as time approaches 100,000 cycles, suggesting.

a steady state response to cyclic loading has not been achieved for the applied stress range used. The transition from CY loading to CR loading in LC1 shows an initial steep recovery in deflection at minimum load that gradually becomes approximately constant at 40 h. Referring to Table 1, the average $\rho_D$ at 40 h is 85 %, and the corresponding 40-hour – to – 100,000 cycle $\rho_D$ ratio is 0.84. The significance is that the deflection growth accumulated during load cycling is not permanent, but on average, about 16 % of it is recovered over the 12 h of creep loading that followed load cycling. Furthermore, noting the flattening trends as 40 h is approached in Figs. 9a and 10a, it is unlikely that more significant deflection recovery would occur had the material been subjected to a longer period of CR loading.

From Fig. 10b and Table 1, the effects of creep loading alone (LC2) show that at 100,000 sonds, deflection has increased on average by 38 %. This compares to the LC1 value of 102 %, which is 2.70 times the LC2 value of 38 %. At 40 h the average LC2 $\rho_D$ has increased slightly from 38 to 41 %. This compares to 85 % for LC1, which is 2.07 times the LC2 value. Extrapolating from the observed trends in Figs. 9b and 10b, LC2 deflection growth is still occurring at 40 h but at a greatly reduced rate. The bearing stiffness of Surlyn ($k_{cyclic}$), is taken as the bearing-stress vs. bearing- strain slope and equal to '$S_{cyclic}$' in Fig. 8 times the total Surlyn thickness of 6.35 mm (3.175 mm each top and bottom). Results for Load Case 1 samples are shown in Fig. 11. The material's bearing stiffness is seen to increase significantly in the first 1000 cycles and thereafter fluctuate only somewhat but with no particular pattern. These fluctuations are likely in response to slight temperature changes that occurred over the 28 h of cyclic loading. At 1000 cycles bearing stiffness

**Table 1**
Normalized deflection data.

| Load Case | Sample | (a) at 100,000 s $\rho_D$ (%) | (b) at 100,000 s $\rho_{D+L}$ (%) | (c) at 40 h $\rho_D$ (%) | (c) / (a) |
|---|---|---|---|---|---|
| LC1 | CY+CR+MF−1 | 128.1 | 87.0 | 102.6 | 0.80 |
| | CY+CR+MF−2 | 87.8 | 60.7 | 76.1 | 0.87 |
| | CY+CR+MF−3 | 108.6 | 67.5 | 89.0 | 0.82 |
| | CY+CR+MF−4 | 98.7 | 64.7 | 86.8 | 0.88 |
| | CY+CR+MF−5 | 94.2 | 60.4 | 77.7 | 0.83 |
| | CY+CR+MF−6 | 93.3 | 58.7 | 80.3 | 0.86 |
| | Average | 102 | 67 | 85 | 0.84 |
| | SD | 14.65 | 10.55 | 9.82 | 0.031 |
| LC2 | CR+MF−1 | 36.8 | na | 40.8 | 1.11 |
| | CR+MF−2 | 36.1 | | 39.9 | 1.11 |
| | CR+MF−3 | 49.5 | | 52.4 | 1.06 |
| | CR+MF−4 | 36.9 | | 40.5 | 1.10 |
| | CR+MF−5 | 29.5 | | 33.0 | 1.12 |
| | Average | 38 | | 41 | 1.10 |
| | SD | 7.24 | | 7.00 | 0.023 |
| LC1/LC2 | Average | 2.70 | | 2.07 | 0.77 |

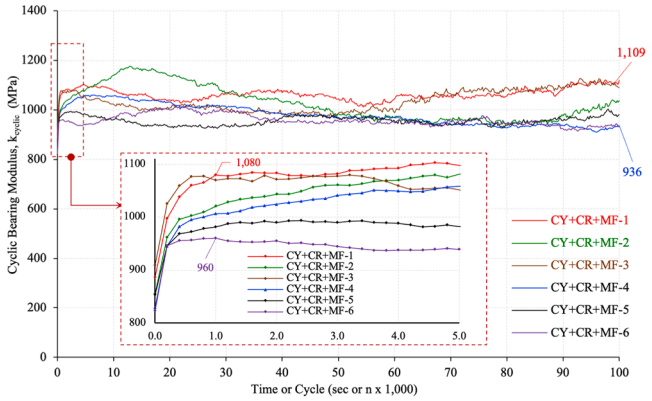


**Fig. 11.** Cyclic bearing modulus.

ranges between 960 and 1080 MPa, with an average of 1020 MPa. At 100,000 cycles, bearing stress is seen to range between about 936 and 1109 MPa, with an average of 1016 MPa. Essentially the bearing stiffness response to cyclic loading reaches a steady state at about 1000 cycles.

### 3.2. Failure test results

Monotonic test-to-failure (MF) results are presented in Figs. 12a, 12b and 12c for Load Cases 1, 2, and 3, respectively. It is understood that before monotonic test-to- failure LC1 samples experienced 100,000 load cycles between 5 and 15 MPa followed by 12 h of creep load at 5 MPa (see Fig. 9a), and LC2 samples experienced 40 h of creep loading at 5 MPa (see Fig. 9b). Load Case 3 sample had no previous load history before test-to-failure. In this way, the effect, if any, of cyclic and creep loading on bearing stiffness and the fracture strength of glass could be assessed. Dur- ing monotonic test-to-failure, all samples were first pre-loaded to an MTS displacement of 0.20 mm and unloaded, to zero load. This was done to settle the sample and load apparatus and engage the displacement instrumentation. The samples were then loaded monotonically under displacement control at a rate of 0.10 mm/minute until glass frac- ture, which was followed by unloading to zero force. The preload, load to fracture and unload phases were continuous and part of a single load and data acquisition protocol. The minor residual displacement at the end of preload phase was subtracted from the.

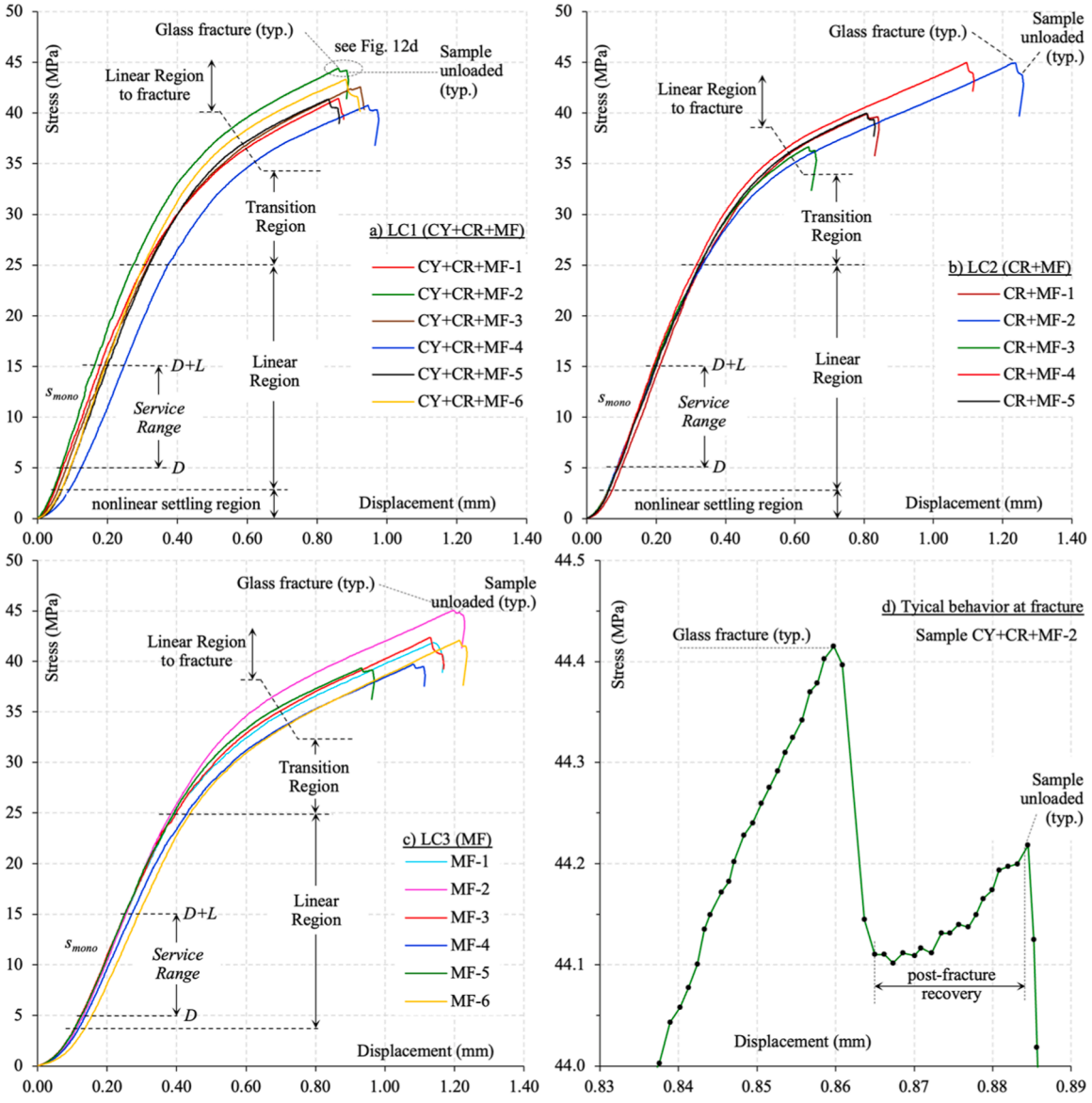


**Fig. 12.** Monotonic failure load-displacement results: a) LC1, b) LC2, c) LC3, d) at fracture.

test results to normalize the slight differences that are specific to each sample.

Referring to Figs. 12a, 12b and 12c, all load cases (LC1, LC2, and LC3) have a similar shape, which can be characterized by an initial nonlinear settling region with increasing stiffness, followed by a linear region that captures the service range, fol- lowed by a nonlinear transition region with decreasing stiffness, and concluding with a second linear region until glass fracture. This quad-mode response shape is the same for all three load cases and shows that cyclic and creep loading do not change the fun- damental response of Surlyn to bearing stress levels at limit states between service and glass fracture.

In general, the first linear region initiates at about 2.5 MPa, representing 0.5D, and ends at about 25 MPa, representing D+ 2 L, or, effectively, the bearing stiffness is approximately constant for a stress range corresponding to 0.5D-to-D+ 2 L. Importantly, this result applies for all three load cases suggesting that load cycling and creep loading does not significantly alter the fundamental bearing response of Surlyn as an interface material. Quantitatively, the service limit state bearing modulus of Surlyn ($k_{mono}$) is calculated as the stress-displacement slope within the service range, which is seen as.

'smono' in Fig. 8, times the total Surlyn thickness of 6.35 mm (again, 3.175 mm each top and bottom), and the results are shown graphically in Fig. 13a. From this data, the monotonic bearing modulus for LC1 and LC2 are very similar, and average 606 and 583 MPa, respectively. However, the monotonic bearing modulus for LC3 is measurably less, with an average value of 505 MPa, or 17 % and 14 % less than LC1 and LC2, respectively. The results show that the bearing modulus is related to load cycling and creep loading. As well, there is little difference in the LC1 and LC2 average bearing moduli, suggesting the load cycling and creep loading have a similar effect on Surlyn bearing modulus under monotonic loading.

Referring to Fig. 12, all samples were loaded to glass fracture, which is shown in exploded form for Sample CY+CR+MF- in Fig. 12d. In general, cracking is charac- terized in the data by a sudden and precipitous drop in load. In general, the load loss at fracture was less than 1 % of that corresponding to fracture. This is followed by a brief recovery where post-fracture load is maintained or increases slightly. To avoid.

an explosive shattering of the glass, the samples were then immediately unloaded. The crack shape was the same in all cases and a typical representation is shown in Fig. 14. As can be seen, the crack had a shell-like shape and initiated on the loaded edge of the column plate and within the 10 mm glass thickness. This orientation suggests the presence of local tensile stresses on the glass surface perpendicular to the crack (Fig. 14c), representing a Mode-I type crack opening. In general, the crack did not penetrate the entire glass height or length (102 mm each), but had an approximate quarter-circle type appearance (Figs. 14a and 14c), penetrating through approximately 40–60 per- cent of the glass depth (shown as ** in Figs. 14a and 14b) and length. The Surlyn surface in contact with the glass had the glass surface texture of the abrasive water jet pattern etched into it, as if a "mold" of the micro surface irregularities was made. As well, the crack pattern was plainly visible on the Surlyn, as can be seen in Fig. 14d. The numerical bearing stress results at glass fracture are shown as a bar chart in Fig. 13b, where the average fracture stress for LC1, LC2, and LC3 is 42.3, 41.3, and 41.8 MPa, respectively. The data clearly shows that the CY loading and CR loading of LC1 and LC2 had no effect on the cracking strength of the glass. This is a significant outcome and shows that there is no correlation between the CY and CR loading applied in this study, and early crack initiation. This was hypothesized to be the case when the experimental program was planned, and to the advantage of Surlyn as an interface material, this hypothesis did not come to fruition. Considering the service stress for D+L of 15 MPa, the average fracture stress of 42 MPa is 2.80 time this service value, which in effect represents an experimental

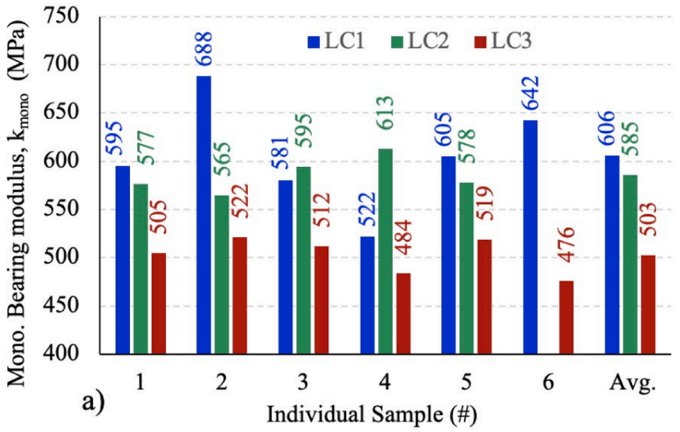


| Sample # | Monotonic Bearing Modulus, $k_{mono}$ (MPa) | | |
|---|---|---|---|
| | LC1 | LC2 | LC3 |
| 1 | 595 | 577 | 505 |
| 2 | 688 | 565 | 522 |
| 3 | 581 | 595 | 512 |
| 4 | 522 | 613 | 484 |
| 5 | 605 | 578 | 519 |
| 6 | 642 | | 476 |
| average | 606 | 585 | 503 |
| min | 522 | 565 | 476 |
| max | 688 | 613 | 522 |
| avg/LC3$_{avg}$ | 1.20 | 1.16 | 1.00 |

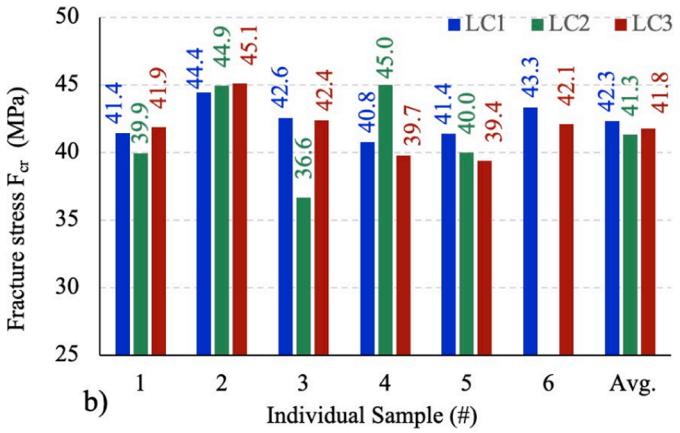


| Sample # | Fracture Stress $F_{cr}$ (MPa) | | |
|---|---|---|---|
| | LC1 | LC2 | LC3 |
| 1 | 41.4 | 39.9 | 41.9 |
| 2 | 44.4 | 44.9 | 45.1 |
| 3 | 42.6 | 36.6 | 42.4 |
| 4 | 40.8 | 45.0 | 39.7 |
| 5 | 41.4 | 40.0 | 39.4 |
| 6 | 43.3 | | 42.1 |
| average | 42.3 | 41.3 | 41.8 |
| min | 40.8 | 36.6 | 39.4 |
| max | 44.4 | 45.0 | 45.1 |
| avg/LC3$_{avg}$ | 1.01 | 0.99 | 1.00 |

**Fig. 13.** Monotonic failure results for a) Bearing modulus, b) Fracture stress.

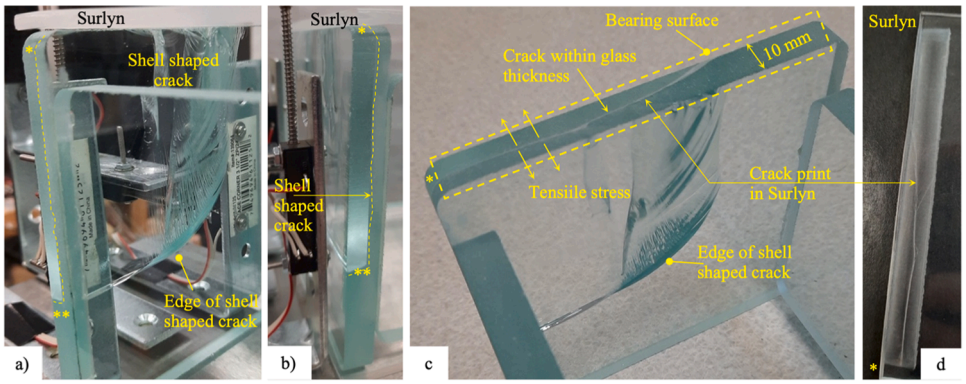


**Fig. 14.** Typical glass fracture photos.

factor-of-safety (FOS) for the limit state of local glass fracture from bearing. This FOS considering all load cases is seen to range from 2.44 to (LC2 Sample 3) to 3.00 (LC2 Samples 2 and 4). Relative to the target bearing stress of 36.6 MPa, which represents an experimental upper bound related to glass failure associated with second-order compression-bending interaction effects from Yost et al. [13], all samples meet or exceed this target. The significance of this result is that the limit-state fracture capacity of glass in bearing with Surlyn exceeds that of limit states related to glass column strength as controlled by flexural buckling. From this result, it is noted that Surlyn effectively allows the strength of glass compression members of normal slenderness to be controlled by column limit states and not by local glass fracture with the interface material.

## 4. Discussion and context of test results

The data presented in Fig. 13 supports directly the objective stated in Section1.2 of developing the flexural buckling strength of hollow glass units (HGU). As was stated in Section 1.2, the compression strength limit state of HGU flexural buckling requires an interface bearing stress in excess of 36.6 MPa. Actually, this magnitude represents an upper bound of multiple HGUs tested in axial compression and failing by flexural buckling (Yost et al., 2021). In specific terms, four individual HGU samples were tested in axial compression and failed by flexural buckling at forces corresponding to bearing stresses of 30.1, 33.7, 33.9 and 36.6 MPa. Importantly here, HGU failure was by the column related limit state of flexural buckling so that the target bearing stress of 36.6 MPa represents an upper bound from Yost et al. (2021) and lower bound in the current study. Thus, the target 36.6 MPa is a conservative magnitude relative to the cited four values.

With this data as context, the results of Fig. 13 show that Surlyn can successfully function as an interface material for compression dominant shell structures constructed using the proposed modular HGU technology. In this context, 'successful' correlates directly to suppressing interface glass cracking and allowing the compression failure limit state of flexural buckling to define the ultimate strength. Moreover, the data of Fig. 13 shows that this minimum bearing stress of 36.6 MPa is achieved in all load cases and therefore not related to the time dependent effects of load cycling and creep considered in this study. In fact, the average bearing stresses of Fig. 13 are well in excess of the target 36.6 MPa, and are seen to be 42.3 MPa for LC1 (CY+CR+MF), 41.3 MPa for LC2 (CR+MF) and 41.8 MPa for LC3 (MF). It can therefore be concluded that for the experimental conditions of the current study, Surlyn will effectively serve the function of preventing local glass fracture due to bearing and by extension allow the full HGU compression strength to be achieved.

The study results of Section 3 also have important meaning in the broader context of transferring bearing stresses in glass and requiring that this be achieved absent of local cracking. To this end, the data of Fig. 13 provides a numerical measure of the cracking strength to be expected for float glass having an abrasive water cut surface and in bearing with Surlyn as an interface material. The data will be of value in a wide range of applications where glass interacts in bearing with other structural materials such as carbon steel, stainless steel, aluminum, and cementitious materials.

## 5. Conclusions

In this research, an experimental program was executed to investigate the behavior of Surlyn when used as an interface material for short glass compression members. An assortment of short glass columns sandwiched between sheets of Surlyn (see Fig. 5) were tested in axial compression to fracture under three different load cases (LC) which include (see Fig. 7): LC1) 100,000-cycle cyclic phase (CY) followed by 12 hr. creep phase (CR) followed by monotonic failure phase (MF), LC2) 40 hr. creep phase (CR) followed by monotonic failure phase (MF), and LC3) Monotonic to failure only phase (MF). From the findings reported in this paper, the following conclusions are made specific to the experimental program executed:

- Cyclic bearing stiffness increases rapidly in about the first 1000 load cycles between bearing stresses of D = 5 MPa and D+L = 15 MPa. Thereafter, the bearing stiffness remains relatively stable until the termination of cyclic loading at 100,000 cycles. The cyclic bearing stiffness range at 1000 and 100,000 load cycles was 960-to-1080 MPa and 936-to-1109 MPa, respectively. Reference for this conclusion is made to Fig. 11.
- The relative increase in deflection between 1 and 100,000 load cycles at mini- mum and maximum load was 102 % and 67 %, respectively. Thus, the rela- tive deflection increase at minimum load was 35 % higher than at minimum load. Reference for this conclusion is made to Fig. 10a and Table 1.
- Samples subjected to 40 h of creep loading at a sustained load of 5 MPa showed an average relative deflection increase at the end of 40 h of 41 per- cent. The relative change in deflection is highly nonlinear, with the majority of the 41 % occurring in the first 5 h. Reference to this conclusion is made to Fig. 10b and Table 1.
- All samples subjected to 100,000 load cycles followed by 12 h of creep loading (Load Case 1) survived with no cracking of the glass column plates. Also, all samples subjected to 40 h of creep loading (Load Case 2) survived with no cracking of the glass column plates.
- Fracture strength of the glass as measured during monotonic testing to failure was unaffected by load history as related to cyclic and creep loading. The average glass fracture strength for samples tested to failure after 100,00 load cycles plus 12 h of creep loading (Load Case 1), 40 h of creep loading (Load Case 2), and no previous cyclic or creep loading (Load Case 3) was 42.3, 41.3 and 41.8 MPa, respectively. Reference to this conclusion to Fig. 13b.

- The target upper bound glass fracture strength of 36.6 MPa was achieved or exceeded by all test samples regardless of load history. As a result, for columns of normal slenderness, when Surlyn is used as an interface material, compression capacity will be limited by column limit states related to flexural buckling and not interface glass cracking. Reference to this conclusion is made to Fig. 13.
- The target bearing strength of 36.6 MPa correlates to a flexural buckling failure limit state for rigid three-dimensional hollow glass compression members, which are proposed for use in modular construction of compression dominant glass shell structures. Thus, it would be expected that full global column strength is achievable before local bearing related fracture limit states occur.
- The bearing stiffness measured in the service load range during monotonic test- ing to failure was influenced by load history. Specifically, the average bearing stiffness in the service load range for samples tested to failure after 100,00 load cycles plus 12 h of creep loading (Load Case 1), 40 h of creep loading (Load Case 2), and no previous cyclic or creep loading (Load Case 3) was 606, 583 and 505 MPa, respectively. Reference to this conclusion is made to Figs. 12 and 13a.
- For all samples, glass fracture occurred in the same way regardless of loading history. At failure, the fracture appeared to resemble a Type I mode crack open- ing with interface tensile stress directed perpendicular to the bearing area in a long direction. Reference to this conclusion is made to Fig. 14c.
- At glass fracture, the samples did not shatter or disintegrate. Rather immedi- ately following glass fracture, there was a precipitous drop in load, followed by a post-fracture recovery where load increased slightly, and finally followed by unloading. In general, the load loss at fracture was less than 1 % of that corresponding to fracture. This behavior at glass fracture was characteristic of all samples. Reference to this conclusion is made to Fig. 12d.

## CRediT authorship contribution statement

**Damon Bolhassani:** Writing – review & editing, Writing – original draft, Validation, Methodology, Conceptualization. **Joseph Robert Yost:** Writing – original draft, Visualization, Validation, Supervision, Resources, Project administration, Methodology, Investigation, Funding acquisition, Formal analysis, Data curation, Conceptualization. **Matthew Cregan:** Methodology, Investigation, Formal analysis. **Yao Lu:** Visualization, Software, Conceptualization. **Masoud Akbarzadeh:** Writing – review & editing, Validation, Supervision, Resources, Project administration, Methodology, Funding acquisition, Conceptualization. **Philipp Amir Chhadeh:** Validation, Methodology, Formal analysis. **Jens Schneider:** Validation, Supervision, Resources, Formal analysis, Conceptualization.

## Declaration of Competing Interest

The authors declare the following financial interests/personal relationships which may be considered as potential competing interests.

Masoud Akbarzadeh reports financial support was provided by National Science Foundation. If there are other authors, they declare that they have no known competing financial interests or personal relationships that could have appeared to influence the work reported in this paper.

## Acknowledgments

This research was supported by the University of Pennsylvania Research Foundation grant (URF), National Science Foundation CAREER AWARD (NSF CAREER- 1944691- CMMI), and the National Science Foundation Future Eco Manufacturing Research Grant (NSF, FMRG-CMMI 2037097) to Dr. Masoud Akbarzadeh. Also, this study was supported by the Villanova University Summer Grant Program (USG) to Dr. Joseph Yost.

## Data Availability

Data will be made available on request.

## References

[1] ArchDaily,Civic center in st germain en laye / atelier 9 portes + philippe harden. ⟨https://www.archdaily.com/29755/civic-center-in-st-germain-philippe-harden⟩, August 20009.
[2] Petersen RI, and Bagger A, Structural use of glass: Cruciform columns and glass portals with bolted connections subjected to bending," in Proceedings Glass Performance Days. Tampere, Finland, pp. 381–385, 2009.
[3] Pocanschi A, Phocas MC. Tragende glasstützen für eine café-bar in göppingen. Bautechnik 2006;83(10):708–14.
[4] van Heugten R, Load bearing glass columns," Master's thesis, Eindhoven University of Technology, Netherlands, 2013.
[5] "Design of glass structures - part 2: Design of out-plane loaded glass compo- nents," no. FprCEN/TS 19100–2:2021 E, 2021.
[6] "Design of glass structures - part 3: Design of in-plane loaded glass components and their mechanical joints," no. FprCEN/TS 19100–3:2021 E, 2021.
[7] JAMAR, Spider glass curtain walls – bolted point fixed glazing ⟨https://www.jamarmalta.com/portfolio-item/spider-glass-curtain-walls-bolted-point-fixed-glazing/⟩, October 2025.
[8] Group, P. Point fixed glass (spider glass)." ⟨https://www.polmek.com/en/point-fixed-glass⟩, October 2025.
[9] 3M™, "3m™ vhb™ structural glazing tape." ⟨https://www.3m.com/3M/en_US/p/d/b40072022/⟩, May 2017.
[10] Akbarzadeh M, Bolhassani M, Nejur A, Yost JR, Byrnes C, Schneider J, Knaack U, Costanzi CB, The design of an ultra-transparent funicular glass structure, pp. 405–413.
[11] Akbarzadeh M, *3D* graphical statics using reciprocal polyhedral diagrams. PhD thesis, ETH Zürich, 2016.
[12] Lu Y, Seyedahmadian A, Chhadeh PA, Cregan M, Bolhassani M, Schnei- der J, Yost JR, Brennan G, Akbarzadeh M. Funicular glass bridge proto- type: design optimization, fabrication, and assembly challenges (Aug) Glass Struc- tures Eng 2022;7:319–30 (Aug).
[13] Yost JR, Bolhassani M, Chhadeh PA, Ryan L, Schneider J, Ak-barzadeh M. Mechanical performance of polyhedral hollow glass units under com- pression. Eng Struct 2022;254:113730.
[14] Yost JR, Cregan M, Bolhassani M, Akbarzadeh M, Lu Y, Chhadeh PA, Schneider J. Experimental investigation of a transparent interface material for glass compression members," Challenging Glass Conference Proceedings, vol. 8, jun 2022.
[15] Sanders K, Bos F, ten Brincke E, Belis J. Edge strength of core drilled and waterjet cut holes in architectural glass (Jun) *Glass Struct Eng* 2021;6:131–45 (Jun).
[16] Wurm J. Glass structures design and construction of self-supporting skins. Berlin, Boston: Birkhäuser, 2007.
[17] Oikonomopoulou F, van den Broek EAM, Bristogianni T, Veer FA, Nijsse R. Design and experimental testing of the bundled glass column (Oct) Glass Struct Eng 2017;2:183–200 (Oct).
[18] Kamarudin MK, Yusoff MM, Disney P, Parke GA. Experimental and numerical investigation of the buckling performance of tubular glass columns under compression. Structures 2018;15:355–69.
[19] Aiello S, Campione G, Minafo G, Scibilia N. Compressive behaviour of laminated structural glass members. Eng Struct 2011;33(12):3402–8.
[20] Kalamar R, Bedon C, Eliašova M. Experimental investigation for the structural performance assessment of square hollow glass columns. Eng Struct 2016;113:1–15.
[21] DOW, "Surlyn™ 8940 ionomer." ⟨https://www.dow.com/en-us/pdp.surlyn-8940-ionomer.1892363z.html#overview⟩, June 2022.s.